Journal of the Chinese Institute of Engineers
Publication details, including instructions for authors and subscription information:
http://www.tandfonline.com/loi/tcie20

# Numerical modeling of displacements due to ocean tide loading: case study at GPS stations in Taiwan and western Pacific

Cheinway Hwanga[a] & J.F. Huang[ab]

[a] Department of Civil Engineering, National Chiao Tung University, 1001 Ta Hsueh Road, Hsinchu 300, Taiwan

[b] Ministry of the Interior, 5 Syujhou Rd., Jhongjheng District, Taipei 100, Taiwan

Published online: 03 Dec 2012.

To cite this article: Cheinway Hwanga & J.F. Huang (2013) Numerical modeling of displacements due to ocean tide loading: case study at GPS stations in Taiwan and western Pacific, Journal of the Chinese Institute of Engineers, 36:8, 1017-1028, DOI: 10.1080/02533839.2012.747045

To link to this article: http://dx.doi.org/10.1080/02533839.2012.747045

*Journal of the Chinese Institute of Engineers*, 2013
Vol. 36, No. 8, 1017–1028, http://dx.doi.org/10.1080/02533839.2012.747045





# Numerical modeling of displacements due to ocean tide loading: case study at GPS stations in Taiwan and western Pacific

Cheinway Hwang[a]* and Jiu-Fu Huang[ab]

[a]*Department of Civil Engineering, National Chiao Tung University, 1001 Ta Hsueh Road, Hsinchu 300, Taiwan;* [b]*Ministry of the Interior, 5 Syujhou Rd., Jhongjheng District, Taipei 100, Taiwan*

(*Received 11 July 2011; final version received 26 June 2012*)

We model the horizontal and radial displacements due to ocean tidal loading (OTL) in a computer program DISOTL (DISplacements due to Ocean Tide Loading). Numerical modeling of OTL considers inner and outer zone contributions. A local tide model and shoreline defined by a GMT and Taiwan digital elevation model is used for the inner zone. OTL-induced displacements from DISOTL, GOTIC2, and BS computer programs differ at the millimeter level in amplitude, but the phase difference can be over 10°. Such displacements at 13 IGS stations in the western Pacific can be up to 8.5 cm in amplitude (KWJ1, Marshall Islands). At stations around Taiwan, the radial displacements can be up to 5.5 cm (MZUM, Matzu Islands). This implies that such large OTL effects (over 1 cm) will have a profound influence on precise global positioning system (GPS) positioning. To establish a new GPS reference frame in Taiwan, the use of a precise computer program is critical. A case study of coastal and offshore-island GPS continuous stations suggests that DISOTL can model OTL corrections to a 1 mm accuracy and reduce coordinate variations by up to 35%.

**Keywords:** DISOTL; GPS; IGS; ocean tide loading; Taiwan

## 1. Introduction

The global positioning system (GPS) is widely used in geodynamic and climate process studies such as plate motion, post glacier rebound, and sea level change. One of the corrections for high-precision (better than 1 cm) GPS applications is displacement due to ocean tide loading (OTL; Baker *et al.* 1995). For example, Dragert *et al.* (2000) found that the maximum radial displacement due to OTL on Canadian coasts is 8 cm. Over the continental shelf of Brittany, OTL causes radial and horizontal displacements up to 12 cm (Melachroinos *et al.* 2008). Dicaprio and Simons (2008) show that the horizontal gradient of OTL-induced displacements can be up to 3 cm per 100 km, which is larger than the expected accuracy in the slope of deformation from InSAR, and can cause a significant error in studying a slow tectonic process. Collilieux *et al.* (2010) suggest that the reference frame realized by geodetic techniques should take into account the OTL effect: with the OTL effects corrected, the results from very long baseline interferometry, GPS, and satellite laser ranging (SLR) can be improved by up to 3.2%, 3.1%, and 1.2%, respectively.

With the deep Pacific Ocean to the east and the shallow Taiwan Strait to the west, the ocean tidal variations in amplitude and phase around Taiwan are large and complicated. As an example, Figure 1 shows the distributions of amplitude and phase of the M2 ocean tide around Taiwan based on the NAO.99jb tide model (Matsumoto *et al.* 2000). The nominal spatial resolution of NAO.99jb is $5' \times 5'$. The amplitude is the largest (about 240 cm) near the southeast China coasts, and decreases toward the south to the South China Sea and east to the Pacific Ocean. Over the Pacific coasts of Taiwan, the amplitude reduces to about 40 cm. As the OTL effect is roughly proportional to tidal amplitude, Figure 1 suggests that the largest and the smallest OTL effects around Taiwan will occur at stations near southeast China coasts and the Pacific Ocean, respectively. Yeh *et al.* (2011) show that, depending on the tide models used, the accuracies of static GPS positioning due to OTL correction at the permanent GPS tracking stations of MOI (Ministry of the Interior, Taiwan) may be improved by 15–36%. The M2 OTL effects at the GPS stations in northwest Taiwan have amplitudes of about 1 cm, while such effects at the offshore islands in the Taiwan Strait are about 1.2–2.7 cm. These effects are significantly larger than the expected accuracies of static GPS positioning. With the increasing popularity of precise point positioning (PPP) in GPS and the increasing demand for PPP accuracy (at cm), a precise OTL computer program for

*Corresponding author. Email: cheinway@mail.nctu.edu.tw

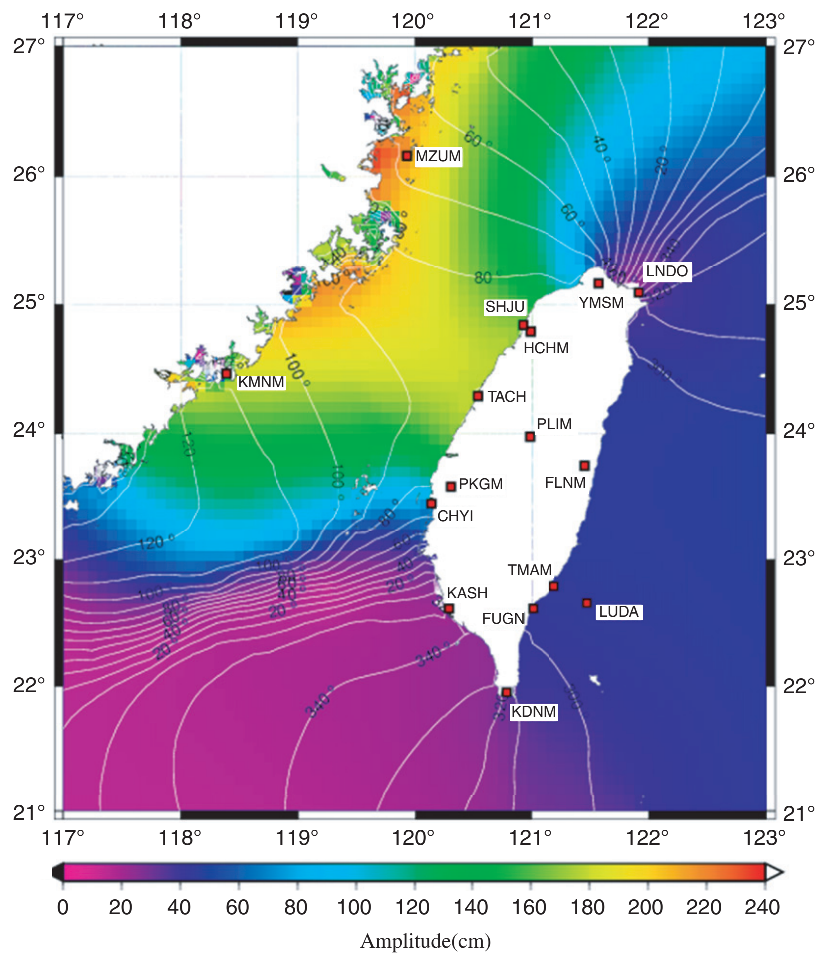


Figure 1. Amplitudes and phases of M2 ocean tide around Taiwan; squares show Taiwan GPS stations for OTL analysis.

correcting GPS positioning results is important and critical.

It is commonly recognized that OTL corrections at coastal GPS stations are less accurate than corrections at stations distant from the sea (Penna *et al*. 2008). Note that the accuracy of the OTL modeling depends on factors such as ocean tide model, coastline and Green's function, with the first being the largest error source. In particular, coasts with complicated shorelines, large tidal amplitudes, and fast phase variations require a precise OTL computer program for precise GPS positioning. Here, our OTL computer program adopts a well-defined shoreline and a high resolution, regional tide model, which substantially improve the OTL modeling accuracy. However, most public OTL computer programs, e.g., SPOTL (Agnew 1996), GOTIC2 (Matsumoto *et al*. 2005), CARGA (Bos and Baker 2005), and BS (Bos and Scherneck 2009, see also http://froste.oso.chalmers.se/loading//index.html), are easy to access and use, but contain less spatial information than regional models. To improve the spatial resolution and accuracy around Taiwan, this article will develop an OTL computer program for horizontal and radial displacements based on a regional tide model and a digital elevation model (DEM) that defines the shoreline of Taiwan. The computer program, called DISplacements due to Ocean Tide Loading (DISOTL), will also take into account station height, which is commonly neglected in global OTL models for displacements. This article will present an analysis of the accuracies of this new model at selected GPS stations in Taiwan and in the western Pacific region, in an attempt to provide critical information for OTL corrections when updating a geodetic reference frame in these regions.

## 2. Displacements due to ocean tide loading: theory

A displacement due to OTL can be expressed as a convolution of global ocean tidal heights and a Green's function. Specifically, in the space domain, the radial, north, and east displacement components due to OTL at any location $p$ are (Farrell 1972, Moritz and Mueller 1987, Lambert 1998, Yang *et al.* 1996)

$$U_r(H_p, \psi_{pq}) = R^2 \rho_w \int\int_D h_q U(H_p, \psi_{pq}) \mathrm{d}\sigma_q, \quad (1)$$

$$U_\theta(H_p, \psi_{pq}) = R^2 \rho_w \int\int_D h_q V(H_p, \psi_{pq}) \cos A \mathrm{d}\sigma_q, \quad (2)$$

$$U_\lambda(H_p, \psi_{pq}) = R^2 \rho_w \int\int_D h_q V(H_p, \psi_{pq}) \sin A \mathrm{d}\sigma_q, \quad (3)$$

where $D$ is the domain of convolution (the entire ocean), $H_p$ the elevation of $p$ (defined as the orthometric height above the geoid), $\psi_{pq}$ the spherical angle between $p$ and a running point at sea, located at $q(\phi_q, \lambda_q)$ with $\phi_q, \lambda_q$ being latitude and longitude, $R$ the mean radius of the Earth, $\rho_w$ the density of seawater $\approx 1030\,\mathrm{kg\,m^{-3}}$, $h_q$ the tidal height above mean sea level, $A$ the azimuth of direction between $p$ and $q$, $\mathrm{d}\sigma_q$ defined as $\mathrm{d}\sigma_q = \cos\varphi_q \mathrm{d}\varphi_q \mathrm{d}\lambda_q$, and the differential surface area on the sphere (in fact only ocean) is $\mathrm{d}S_q = R^2 \mathrm{d}\sigma_q$.

Here, $U(H_p, \psi_{pq})$ and $V(H_p, \psi_{pq})$ are Green's functions for the radial and horizontal displacements due to OTL. In this article, we extend the Green's functions $U$ and $V$ to take into account station height. The expressions of $U$ and $V$ are (see the derivations in Appendix)

$$U(H_p, \psi_{pq}) = \frac{R}{M}\left[\frac{h'_\infty \sigma}{\sqrt{1 - 2\sigma\cos\psi_{pq} + \sigma^2}} + U'(H_p, \psi_{pq})\right], \quad (4)$$

$$V(H_p, \psi_{pq}) = \frac{R}{M}\left[\frac{-l'_\infty \sigma^2 \sin\psi_{pq}}{\left(1 - 2\sigma\cos\psi_{pq} + \sigma^2\right)^{3/2}} + V'(H_p, \psi_{pq})\right], \quad (5)$$

$$U'(H_p, \psi_{pq}) = \sum_{n=0}^{N} \sigma^{n+1}(h'_n - h'_\infty) P_n(\cos\psi_{pq}), \quad (6)$$

$$V'(H_p, \psi_{pq}) = \sum_{n=1}^{N} \sigma^{n+1}(l'_n - l'_\infty) \frac{\mathrm{d}P_n(\cos\psi_{pq})}{\mathrm{d}\psi}, \quad (7)$$

where

$M$ is the mean mass of the Earth, $h'_n, l'_n$ the loading Love numbers of degree $n$, and $P_n(\cos\psi)$ Legendre function of degree $n$.

The factor $\sigma = \frac{R}{R+H_p}$ is attenuated by the station height $H_p$. We adopt the loading Love numbers $h'_n, l'_n$ of Farrell (1972) to compute the Green's functions $U$ and $V$ based on Equations (4)–(7) (Appendix). In addition, our numerical computer program (see Section 3.1) can accept user-defined loading Love numbers. The height-dependent formulae for OTL displacements in Equations (4)–(7) are presented for the first time. Height-dependent Green's functions for the atmospheric loading effect and OTL-induced gravity effect have been presented by Guo *et al.* (2004), Hwang and Huang (2012).

In general, the Green's functions for displacements in global computer programs such as GOTIC2 and BS do not consider station height. That is, station height is set to 0 in the computer programs. To see the effect of station height, we compute the difference between the radial OTL displacements (due to M2, S2, N2, K2, K1, O1, P1, Q1, MF, MM, and SSA ocean tide) at sea level and at a given station height as a function of station height for GPS stations MZUM around Taiwan (Figure 1). The radial OTL displacement at sea level is 5.8 cm for MZUM. If the elevation of MZUM was 500 m and we regarded the elevation as zero (sea level), we would have committed a relative error of 0.26 ppm. It is estimated that (based on DISOTL, see Section 3.1), for a station at a high elevation around Taiwan, e.g., station Mt. Jade (Yu Shan; height 3952 m), neglecting the station height in the Green's function can cause an error of more than 1 mm.

## 3. Numerical modeling of OTL displacement: DISOTL

### 3.1. *Model development*

In the numerical modeling of OTL-induced displacements, we expand the displacements into Fourier series in the same way as the Fourier expansions of tidal height (Foreman and Henry 1979, Hwang and Huang 2012). A constituent of displacement has the same frequency as the ocean tide counterpart, with a different phase. For a given OTL constituent and a given location, we first convolve the global tide of the same constituent with the Green's functions to obtain the amplitude and phase of the OTL constituent. The OTL effect at any time is then evaluated using the amplitude and phase in exactly the same way as the Fourier series expansion of the ocean tide.

In this article, we use the same numerical integration approach as that used in the development of the OTL gravity effect (Hwang and Huang 2012). Specifically, for a given geographic location (latitude, longitude, and station height), Equation (1) is implemented using numerical integration (this process is called numerical convolution) to obtain the amplitudes and phases of given OTL constituents. The OTL computer program developed in this article is called DISOTL. The numerical convolution is divided into inner and outer zone integrations, with a regional tide model for the former and a global tide model for the latter. The optimal sizes of the inner and outer zones follow Hwang and Huang (2012). Around Taiwan, we choose to use the regional tide model of Hu *et al.* (2010), which assimilates all tide gage records in the model. The global tide model NAO.99 b (Matsumoto *et al.* 2000) is adopted for the outer zone. NAO.99 b blends tide gage data with satellite altimetry data in the model, and it best fits the tidal records in the western Pacific region (Huang *et al.* 2008, Hwang *et al.* 2009). The model of Hu *et al.* (2010) gives tidal amplitudes and phase on a $5' \times 5'$ grid. In a comparison between modeled and *in situ* tidal heights, the root mean square (RMS) difference for M2 is 5.1 cm, which is significantly smaller than the RMS difference between NAO.99 b and the *in situ* records from the same tide gages for comparison. In addition, DISOTL uses the shoreline defined by the full-resolution landmask of GMT (for coastal areas not around Taiwan) and the new DEM of Taiwan (shoreline corresponds to zero elevation). The new DEM was generated in 2008 and is available by application at https://dtm.gps.moi.gov.tw/dtm/dtm/index.aspx.

Figure 2 shows the distributions of amplitudes and phases of displacement components due to M2 ocean tides around Taiwan and southeast China coasts. In general, the radial component has the largest amplitude, followed by the east component and then the north component. The patterns of amplitude and phase distributions of the radial component are similar to those of the OTL gravity effect (Hwang and Huang 2012). Also, the radial component is the largest near the southeast China coasts and the smallest along the Central Range of Taiwan. By contrast, the pattern of the east component is significantly different from that of the radial component. In particular, the east component is the largest along the Central Range and diminishes toward the Taiwan Strait and the Pacific Ocean. This is probably caused by the sharp differences in amplitude and phase between the ocean tides in the Taiwan Strait and the Pacific Ocean (Figure 1). Also, the differences of the ocean tides between the western and eastern oceanic regions of Taiwan create large gradients of displacement in the east component. Over Penghu Island, a high in the north component exists, and this high lies roughly in the northeast–southwest direction. The amplitude of the north component on mainland China is rather small (less than 1 mm). In general, the phase variations of the east and north components are relatively smooth compared to that of the radial component.

### 3.2. *Model comparison*

DISOTL is compared with two other OTL displacement computer programs, GOTIC2 and BS. BS is available through the internet (http://froste.oso.chalmers.se/loading//index.html) and allows users to choose among several global ocean tide models to compute OTL. Similar to DISOTL, GOTIC2 uses NAO.99Jb and NAO.99 b, respectively, for the inner and outer zones. Table 1 compares the modeled amplitudes and phases of the eight leading OTL constituents (M2, S2, N2, K2, K1, O1, P1, and Q1) around Taiwan from DISOTL, GOTIC2, and BS at station HCHM. For the eight constituents, the largest difference in the radial amplitude between DISOTL and GOTIC2 is about 0.06 cm (K1) and is about 0.05 cm (M2) between DISOTL and BS. The largest difference in phase between DISOTL and GOTIC2 occurs in the north component and is about $12^\circ$ (N2). The largest difference between DISOTL and BS again occurs in N2 and is $11^\circ$.

Table 2 repeats the comparison among the three computer programs at station MZUM, where the ocean tide and the radial displacement are the largest compared to other regions in Figure 1. For the eight constituents at MZUM, the largest difference in amplitude between DISOTL and GOTIC2 is 0.08 cm in the north component (M2), and the largest difference between DISOTL and BS is 0.12 cm in the radial component (M2). Also, the largest phase difference between DISOTL and GOTIC2 is $37^\circ$ (K2) in the north component, and the largest phase difference between DISOTL and BS is $32^\circ$ (K2) in the north component. Tables 1 and 2 suggest that the differences in amplitude among DISOTL, GOTIC2, and BS computer programs are below 1 mm, but the differences in phase can reach tens of degrees.

## 4. OTL-induced displacements at selected IGS and Taiwan stations in the western Pacific

### 4.1. *IGS stations*

We select 13 IGS stations (two in Taiwan) to assess OTL-induced displacements. Figure 3 shows the distribution of amplitudes and phases of the M2 ocean tide (NAO99b) and the locations of the IGS stations. In general, the amplitude increases with decreasing ocean depth. Over the continental shelves of the western Pacific, Thailand and Burma, the tidal amplitude can be over 1 m. The amplitudes in the South China Sea and the Sea of Japan are about half the size of the amplitudes in the western Pacific Ocean. Such a rapid change in the west–east direction will lead to large gradients in the horizontal displacements as in the case of Taiwan. In the present comparison, we extend

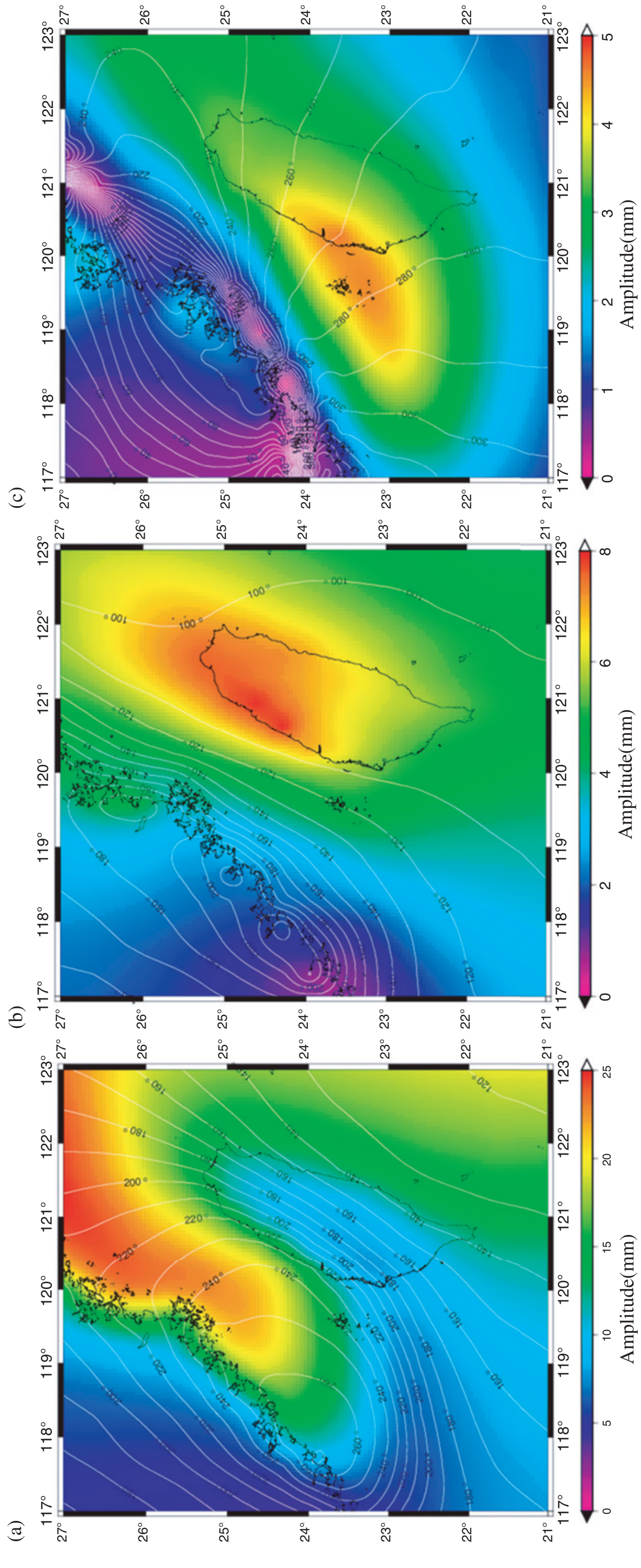


Figure 2. Amplitudes and phases of displacements due to M2 ocean tide in the radial (a), east (b), and north (c) components.

Table 1. Amplitudes and phases of displacements from computer programs DISOTL, GOTIC2, and BS at station HCHM (Hsinchu).

| | Radial | | | East | | | North | | |
|---|---|---|---|---|---|---|---|---|---|
| Tide | DISOTL | GOTIC2 | BS | DISOTL | GOTIC2 | BS | DISOTL | GOTIC2 | BS |
| M2 | 1.27 [a] | 1.31 | 1.22 | 0.79 | 0.81 | 0.81 | 0.36 | 0.39 | 0.38 |
| | −148 [b] | −148 | −149 | 102 | 104 | 104 | −109 | −108 | −107 |
| S2 | 0.32 | 0.31 | 0.29 | 0.29 | 0.29 | 0.29 | 0.13 | 0.14 | 0.14 |
| | −133 | −129 | −132 | 126 | 129 | 129 | −83 | −81 | −80 |
| N2 | 0.26 | 0.29 | 0.27 | 0.15 | 0.15 | 0.15 | 0.06 | 0.07 | 0.06 |
| | −169 | −172 | −175 | 99 | 91 | 92 | −112 | −124 | −123 |
| K2 | 0.07 | 0.08 | 0.07 | 0.08 | 0.08 | 0.08 | 0.04 | 0.04 | 0.04 |
| | −132 | −135 | −140 | 127 | 124 | 125 | −81 | −84 | −84 |
| K1 | 0.90 | 0.96 | 0.94 | 0.24 | 0.25 | 0.26 | 0.13 | 0.12 | 0.13 |
| | −70 | −71 | −71 | −135 | −134 | −133 | 179 | 178 | 175 |
| O1 | 0.79 | 0.83 | 0.82 | 0.16 | 0.17 | 0.17 | 0.12 | 0.11 | 0.13 |
| | −95 | −93 | −93 | −158 | −156 | −156 | 148 | 144 | 143 |
| P1 | 0.30 | 0.31 | 0.31 | 0.08 | 0.08 | 0.08 | 0.04 | 0.04 | 0.04 |
| | −73 | −73 | −73 | −137 | −135 | −135 | 178 | 175 | 172 |
| Q1 | 0.16 | 0.18 | 0.17 | 0.03 | 0.03 | 0.03 | 0.03 | 0.02 | 0.03 |
| | −104 | −100 | −99 | −177 | −168 | −166 | 133 | 130 | 128 |

Note: [a]Amplitude (in cm) and [b]Greenwich phase lag (in degree), $\pm 180^\circ$.

Table 2. Amplitudes and phases of displacements from computer programs DISOTL, GOTIC2, and BS at station MZUM (Matzu).

| | Radial | | | East | | | North | | |
|---|---|---|---|---|---|---|---|---|---|
| Tide | DISOTL | GOTIC2 | BS | DISOTL | GOTIC2 | BS | DISOTL | GOTIC2 | BS |
| M2 | 2.32 [a] | 2.35 | 2.20 | 0.39 | 0.42 | 0.40 | 0.07 | 0.15 | 0.11 |
| | −132 [b] | −134 | −131 | 161 | 171 | 164 | 120 | 107 | 105 |
| S2 | 0.69 | 0.68 | 0.65 | 0.13 | 0.13 | 0.13 | 0.03 | 0.03 | 0.03 |
| | −108 | −105 | −102 | 173 | 176 | 177 | −156 | −164 | −177 |
| N2 | 0.40 | 0.46 | 0.44 | 0.08 | 0.09 | 0.09 | 0.02 | 0.03 | 0.02 |
| | −142 | −158 | −158 | 149 | 163 | 147 | 93 | 71 | 70 |
| K2 | 0.18 | 0.18 | 0.17 | 0.03 | 0.03 | 0.04 | 0.01 | 0.01 | 0.01 |
| | −101 | −109 | −108 | 169 | 176 | 170 | −142 | −179 | −174 |
| K1 | 0.95 | 0.99 | 0.97 | 0.25 | 0.26 | 0.27 | 0.18 | 0.18 | 0.19 |
| | −72 | −72 | −72 | −111 | −108 | −110 | 162 | 157 | 158 |
| O1 | 0.81 | 0.83 | 0.82 | 0.18 | 0.19 | 0.19 | 0.15 | 0.16 | 0.17 |
| | −98 | −95 | −95 | −134 | −151 | −132 | 130 | 125 | 127 |
| P1 | 0.31 | 0.32 | 0.31 | 0.08 | 0.08 | 0.09 | 0.06 | 0.06 | 0.06 |
| | −74 | −74 | −75 | −112 | −110 | −112 | 159 | 154 | 156 |
| Q1 | 0.17 | 0.18 | 0.18 | 0.03 | 0.04 | 0.04 | 0.03 | 0.03 | 0.04 |
| | −108 | −102 | −100 | −148 | −140 | −141 | 116 | 114 | 117 |

Note: [a]Amplitude (in cm) and [b]Greenwich phase lag (in degree), $\pm 180^\circ$.

the tidal components to cover 11 leading tides (M2, S2, N2, K2, K1, O1, P1, Q1, MF, MM, and SSA) and compute the summed amplitude of the 11 constituents as

$$A^n = \sum_{j=1}^{11} a_j^n, \qquad (8)$$

where $j = 1, \ldots, 11$, represent M2, S2, N2, K2, K1, O1, P1, Q1, MF, MM, and SSA, $n$ the station number and $a_j^n$ the amplitude of the $j$th constituent. The contribution of an individual constituent (amplitude) to $A^n$ is shown in Figure 4(a). The 11 leading OTL constituents contribute 95.5% of the total amplitude at TNML, which is near the Hsinchu SG station (Hwang *et al.* 2009).

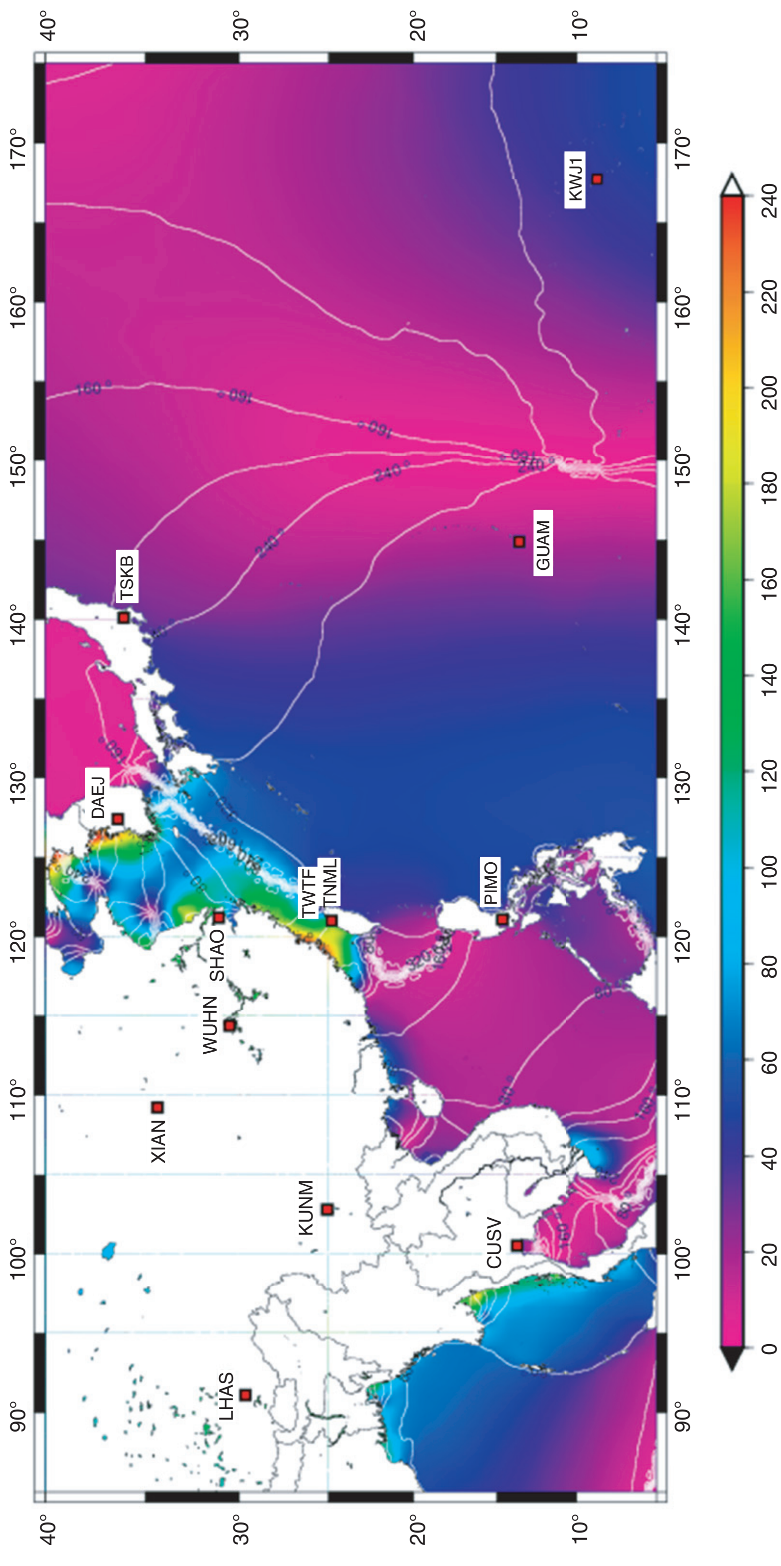


Figure 3. Distribution of M2 ocean amplitudes and phases in the western Pacific; squares show the selected IGS stations.

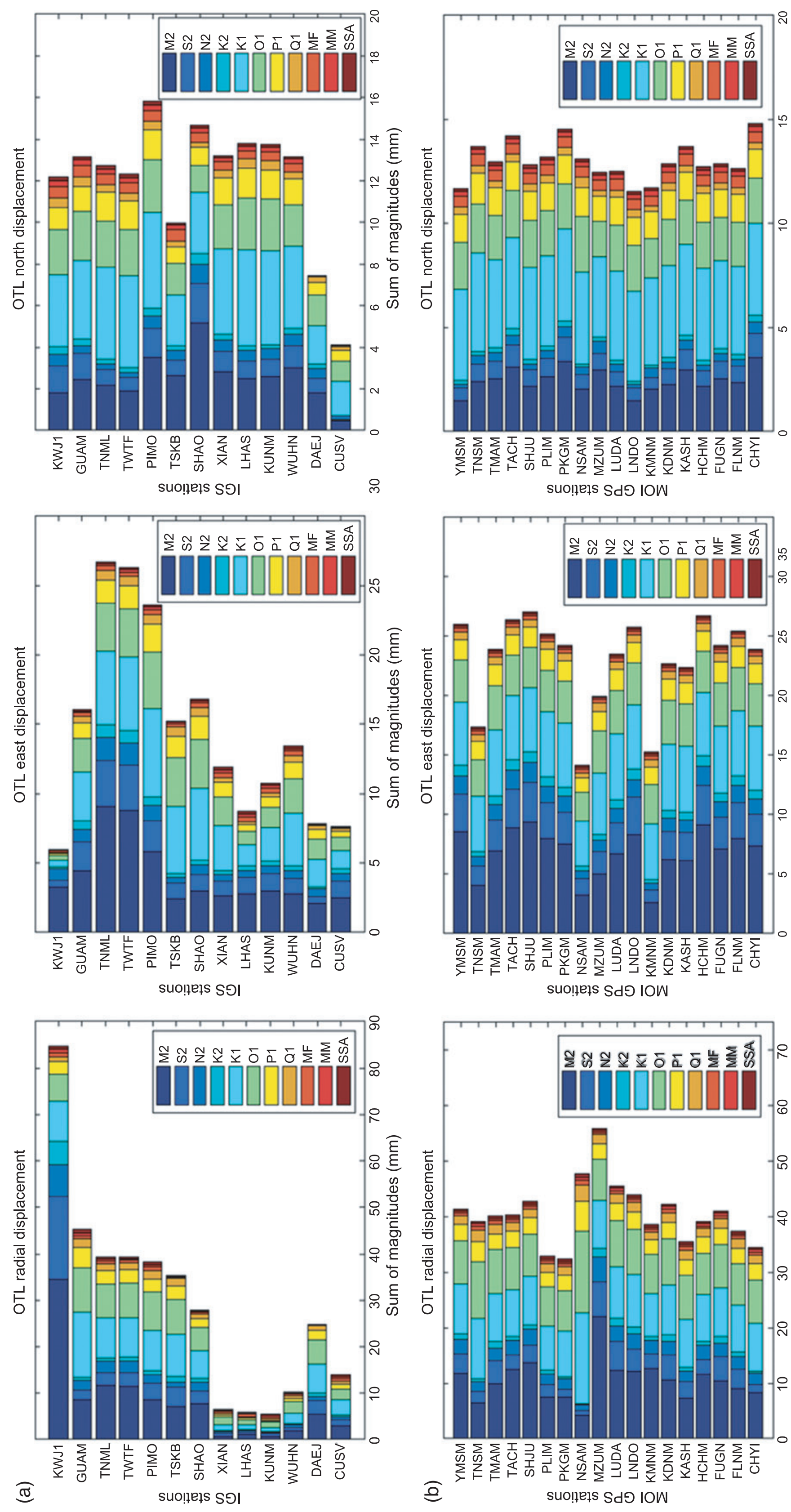


Figure 4. The amplitudes of the 11 constituents of OTL displacement at: (a) 13 IGS stations in the western Pacific and (b) GPS stations in Taiwan.

Below is a summary of the modeled displacements based on Figure 4(a):

(1) Radial component

The radial displacement at KWJ1 (around Marshall Islands) is the largest, despite the fact that it is situated over the deep ocean with relatively small ocean tides. In particular, the amplitude of the M2 radial displacement at KWJ1 is 3.5 cm, which is larger than the amplitude 2.3 cm at Matzu (Table 2) where the amplitude of the M2 ocean tide is 2.4 m. The sum of the 11 amplitudes reaches 8.5 cm at KWJ1, which is the largest among the 13 IGS stations. The sum is about 4 cm at TWTF and TNML in Taiwan, PIMO in the Philippines, and TSKB in Japan, which are stations surrounded by seas. The sums at SHAO (coastal China), DAEJ (Korea) are about 3 cm, followed by 1.5 cm at CUSV (Thailand), 1 cm at WUHN (inland China). The sums at the inland stations XIAN, LHAS, and KUNM are about 0.5 cm and are the smallest.

(2) East component

The M2 amplitudes at TWTF and TNML (Taiwan) in the east component reach 1 cm, and the summed amplitudes of the 11 tides are about 2.7 cm. The east components at these two stations are the largest among the 13 stations, followed by PIMO (2.5 cm), SHAO, GUAM, and TSKB (1.5–2.0 cm), and then WUHN, KUNM, and XIAN (1.0–1.5 cm). The amplitudes at other stations are about 0.6–1.0 cm.

(3) North component

The amplitudes of K1 and O1 at PIMO are the largest, with the summed amplitude being 1.6 cm here. The summed amplitude at SHAO is 1.5 cm, followed by LHAS, KUNM, WUHN, XIAN, GUAM, TWTF, TNML, and KWJ1 (1.2–1.4 cm), TSKB (1.0 cm), DAEJ (0.8 cm), and then CUSV (0.4 cm).

Of the 13 stations, the largest displacement occurs in the radial component (largest 8.5 cm at KWJ1), followed by the east component (largest 2.7 cm at TNML), and finally the north component (largest 1.6 cm at PIMO). As stated before, the vast open ocean around KWJ1 creates a major radial displacement here. The large gradient of tidal amplitudes from the shallow waters of the Taiwan Strait to the deep waters off the eastern Taiwan coast creates the largest east component at TNML. However, the east component at KWJ1 is only 0.6 cm, which is significantly smaller than the radial component here. Also, the radial component at WUHN is 1.0 cm, which is smaller than the east and north components. For inland stations like WUHN, the radial displacement decreases with increasing distance to the sea, but the variation in the horizontal displacement may not follow such a rule. The analysis presented in this section suggests that the OTL-induced displacement does not necessarily depend on the proximity of a station to the sea. Therefore, it is highly important to use a precise OTL computer program to account for the displacement effect when establishing a national coordinate reference frame by geodetic techniques such as GPS and SLR. Also, if the length of a GPS observing session for relative positioning is not sufficiently long, it will be difficult to remove the OTL displacement effects at the semi-diurnal and diurnal bands (Penna *et al.* 2007), making the GPS accuracy degraded. Because it is flexible enough to incorporate new DEM and tide models, DISOTL can be regularly improved to meet the need of an increasing positioning accuracy in the case of using multiple satellite navigation systems including GPS, GLONASS, and GALILEO.

### 4.2. *Taiwan GPS stations*

As shown in Figure 1, the amplitude of M2 is the largest near the southeast China coast and decreases toward the Pacific Ocean. The amplitudes of M2 ocean tide range from about 0.4 m to over 2 m. Such a large tidal variation may also give rise to a large variation in the OTL-induced displacement around Taiwan. In this section, we have computed the summed amplitudes using Equation (6) at 18 MOI-operated GPS continuous stations around Taiwan (Figure 1), and the result is shown in Figure 4(b). Stations TNSM and NSAM are located in Dongsha Atoll and Nansha Island in the South China Sea, respectively, and are not shown in Figure 1. The largest radial displacement (M2) of 2.0 cm is found at MZUM, where the M2 ocean tidal amplitude is also the largest. The summed amplitude at MZUM is 5.5 cm and is the largest among the 18 stations. The summed radial amplitudes at other stations range from 3.0 to 4.5 cm, with the smallest amplitudes being at PLIM and PKGM. For the east component, the summed amplitudes range from 2.0 to 2.7 cm and the smallest amplitudes occur at KMNM and NSAM. For the north component, the summed amplitudes range from 1.2 to 1.5 cm, with the largest amplitudes being at CHYI and PKGM.

Like the IGS stations (Section 4.1), Figure 4(b) suggests that on average the radial displacement is the largest, followed by the east displacement and then the north displacement. The results from Figures 2 and 4 are quite consistent in the distribution of M2 amplitudes. Over a large land mass such as mainland China, in general the radial displacement due to OTL will diminish toward inland areas (Figure 2).

Table 3. RMS values (in cm) of coordinate variations with/without OTL correction at stations HCHM, MZUM, and KMNM.

| Station | w/o[a] | DISOTL[b] | GOTIC2 | BS |
|---|---|---|---|---|
| HCHM | 2.96 | 2.03 | 2.04 | 2.05 |
| MZUM | 3.00 | 1.95 | 1.97 | 1.99 |
| KMNM | 3.01 | 2.49 | 2.50 | 2.52 |

Notes: [a]Without OTL correction and [b]correction using modeled OTL by DISOTL (same for GOTIC2 and BS).

However, because Taiwan is surrounded by seas and its area is relatively small (about 36,000 $km^2$), the reduction of the OTL effect by moving inland is small. As such, even the smallest radial displacements at PLIM and PKGM reach 3.0 cm (summed amplitude). In the open ocean, the summed radial displacements at TNSM and NSAM are 4.0 and 4.8 cm, respectively, which are smaller than the amplitude of 8.5 cm at KWJ1 in the open Pacific Ocean. Again, it is important to use a precise computer program when correcting for the OTL displacements in GPS data processing.

A further modeling comparison was made using about 1 week of GPS observations in 2005 and 2008 at HCHM, MZUM, and KMNM. These stations are within a few kilometer of the sea (see the distance to sea in Table 3). Mean coordinates in a 3 h session (follow Yeh *et al.* 2011) at HCHM, MZUM, and KMNM were determined using relative positioning to the IGS station WUHN. Because the three stations experience very small plate motions (at sub-mm/year level), the variations in the coordinates are affected mostly by GPS positioning accuracy, plus environmental corrections that include the corrections due to OTL displacements. The range of radial displacements at HCHM based on DISOTL is 6.0 cm, which is larger than the summed amplitude (4.0 cm) in Figure 4(b). Table 3 presents the RMS coordinate variations of the 3 h mean coordinates with and without OTL corrections. As expected, the variations without OTL corrections are larger than the variations with such corrections. Corrections with DISOTL, GOTIC2, and BS result in similar RMS variations, but DISOTL yields the smallest variation. At HCHM, MZUM, and KMNM, correcting the OTL effect reduces the variations by 31%, 35%, and 17%, respectively.

## 5. Conclusions and suggestions

This article shows the theory of OTL-induced displacements and presents a DISOTL that models such displacements. Height-dependent Green's functions are introduced. Such a station-height effect can be over 1 mm for GPS stations at high elevations in Taiwan and the world. The comparisons of eight leading OTL displacement components from DISOTL, GOTIC2, and BS at stations HCHM and MZUM show that DISOTL performs equally well as the two well known global computer programs. In the 1 year (2008) comparison, the RMS difference between the modeled displacement of DISOTL and those of GOTIC2 and BS is about 1 mm, with the maximum difference being 2 mm. The horizontal displacements due to OTL at some of the IGS stations can exceed 1 cm. Over Taiwan, the station with the largest radial displacement is MZUM (5.5 cm). At PLIM, which is tens of kilometers away from the ocean, the range of OTL-induced radial displacements is over 3 cm. Such large OTL effects (over 1 cm) will have a profound influence on the newly popular technique of PPP in GPS. This article (mainly Table 3) suggests that correcting the OTL effect in GPS positioning can reduce the coordinate variations by up to 35%.

With increasing positioning accuracy from the use of multiple satellite navigation systems, a precise computer program for correcting OTL-induced displacements becomes critically important. If the geodetic reference frame of a country is to be updated using multiple satellite navigation systems, an up-to-date OTL computer program should be used in the project of reference coordinate updating, and validations should be made to confirm the claimed modeling accuracy. For Taiwan, the variation of OTL with respect to location is large (up to a few cm over all of Taiwan), thus relative positioning of GPS cannot necessarily reduce the OTL effects to a desired accuracy through the cancelation of 'common-mode' errors. In this regard, a precise OTL for the e-GPS system of Taiwan is important. Also, PPP does stand-alone positioning, so it requires an even more precise OTL computer program than the relative positioning (Yuan *et al.* 2009).

**Acknowledgments**

This study was supported in part by the Ministry of the Interior of Taiwan, under the project 'Establishment and maintenance of gravity datum', and in part by the National Science Council of Taiwan, under grant no.99-2923-M-009-002.

**Nomenclature**

$\psi_{pq}$ Spherical angle between $p$ and $q$ (arc degree)

$A$ Azimuth of direction (arc degree)
$H$ Orthometric height (m)
$h_q$ Tidal height above mean sea level (m)
$M$ Mean mass of the Earth (kg)
$R$ Mean radius of the Earth (m)
$\rho_w$ Density of seawater (kg m$^{-3}$)
$U$ Green's function for the radial displacement due to OTL
$V$ Green's function for the horizontal displacement due to OTL
$l'_n$ Loading Love number for the horizontal displacement
$h'_n$ Loading Love number for the radial displacement
$a_j^n$ Amplitude of the tidal constituent (mm)
$P_n(\cos\psi)$ Legendre function

## References


Agnew, D.C., 1996. *SPOTL: some programs for ocean-tide loading*. La Jolla, CA: Scripps Institution of Oceanography, Reference Series 96–98, 35.

Baker, T.F., Curtis, D.J., and Dodson, A.H., 1995. Ocean tide loading and GPS. *GPS world*, 6 (3), 54–59.

Bos, M.S. and Baker, T.F., 2005. An estimate of the errors in gravity ocean tide loading computations. *Journal of geodesy*, 79 (13), 50–63.

Bos, M.S. and Scherneck, H.G., 2009. *Web page for obtaining ocean tide loading corrections* [online]. Available from: http://froste.oso.chalmers.se/loading//index.html [Accessed 30 March 2012].

Collilieux, X., *et al.*, 2010. Impact of loading effects on determination of the international terrestrial reference frame. *Advances in space research*, 45 (1), 144–154.

Dicaprio, C.J. and Simons, M., 2008. Importance of ocean tidal load corrections for differential InSAR. *Geophysical research letters*, 35 (22), L22309.

Dragert, H., James, T.S., and Lambert, A., 2000. Ocean loading corrections for continuous GPS: a case study at the Canadian coastal site Holberg. *Geophysical research letters*, 27 (14), 2045–2048.

Farrell, W.E., 1972. Deformation of the Earth by surface loads. *Reviews of geophysics and space physics*, 10 (3), 761–797.

Foreman, M.G.G. and Henry, R.F., 1979. *Tidal analysis based on high and low water observations*. Pacific marine science report, Patricia Bay: Institute of Ocean Sciences.

Guo, J.Y., *et al.*, 2004. Green's function of the deformation of the Earth as a result of atmospheric loading. *Geophysical journal international*, 159 (1), 53–68.

Hu, C.K., *et al.*, 2010. Numerical simulation of barotropic tides around Taiwan. *Terrestrial, atmospheric and oceanic sciences*, 21 (1), 71–84.

Huang, J.F., Hwang, C., and Jan, S., 2008. Modeling gravity effect of ocean tidal loading around Taiwan: accuracy assessment using FG5 and superconducting gravity data, Abstract G41A-02, *Eos transactions, American geophysical union. In: Western Pacific geophysics meeting supplies*, 29 July–1 August 2008, Cairns, Australia.

Hwang, C. and Huang, J.F., 2012. SGOTL: a computer program for modeling high-resolution, height-dependent gravity effect of ocean tide loading. *Terrestrial, atmospheric and oceanic sciences*, 23 (2), 219–229.

Hwang, C., *et al.*, 2009. Results from parallel observations of superconducting and absolute gravimeters and GPS at the Hsinchu station of Global Geodynamics Project, Taiwan. *Journal of geophysical research,* 114, B07406.

Lambert, A., *et al.*, 1998. Improved ocean tide loading corrections for gravity and displacement: Canada and northern United States. *Journal of geophysical research*, 103 (B12), 30 231–30244.

Matsumoto, K., Takanezawa, T., and Ooe, M., 2000. Ocean tide models developed by assimilating TOPEX/POSEIDON altimeter data into hydrodynamical model: a global model and a regional model around Japan. *Journal of oceanography*, 56 (5), 567–581.

Matsumoto, K., *et al.*, 2005. GOTIC2: a program for computation of oceanic tidal loading effect. *Journal of the geodetic society of Japan*, 47 (1), 243–248.

Melachroinos, S., *et al.*, 2008. Ocean tide loading (OTL) displacements from global and local grids: comparisons to GPS estimates over the shelf of Brittany, France. *Journal of geodesy*, 82 (6), 357–371.

Moritz, H., 1980. *Advanced physical geodesy*. Karlsruhe, Germany: Wichmann.

Moritz, H. and Mueller, I.I., 1987. *Earth rotation: theory and observation*. New York: Unger.

Penna, N.T., King, M.A., and Stewart, M.P., 2007. GPS height time series: short-period origins of spurious long-period signals. *Journal of geophysical research*, 112 (2), B02402.

Penna, N.T., *et al.*, 2008. Assessing the accuracy of predicted ocean tide loading displacement values. *Journal of geodesy*, 82 (12), 893–907.

Yang, Z., *et al.*, 1996. Comprehensive ocean loading parameters of sites in East Asia with spherical harmonic method. *In*: J. Segawa, H. Fujimoto and S. Okubo, eds. *The international symposium on gravity, geoid and marine geodesy, International association of geodesy symposia, 30 September–5 October 1996, Tokyo*. Vol. 117, New York: Springer, 9343–9350.

Yeh, T.K., *et al.*, 2011. Vertical displacement due to ocean tidal loading around Taiwan based on GPS observations. *Terrestrial, atmospheric and oceanic sciences*, 22 (4), 373–382.

Yuan, L.G., *et al.*, 2009. Estimates of ocean tide loading displacements and its impact on position time series in Hong Kong using a dense continuous GPS network. *Journal of geodesy*, 83 (11), 999–1015.

## Appendix

### *Green's functions for OTL-induced displacements*

The notations used here are exactly the same as those used in the text, except for a few occasions. For degree $n \geq N$, where $N$ is a sufficiently large number, the variation of $h'_n$ is asymptotically small, and we can assume the loading Love numbers are a constant with $h'_n = h'_\infty$. Based on the concept of the potential external to the Earth (Moritz and Muller 1987) and the concept of surface mass loading (Farrell 1972), the Green's function for the radial component considering station height is

$$U(H_p, \psi_{pq}) = \frac{R}{M}\sum_{n=0}^{\infty}\sigma^{n+1}h'_n P_n(\cos\psi_{pq}), \\ = \frac{R}{M}\left[\sum_{n=0}^{N}\sigma^{n+1}h'_n P_n(\cos\psi_{pq}) + h'_\infty \sum_{n=N+1}^{\infty}\sigma^{n+1}P_n(\cos\psi_{pq})\right], \quad \text{(A.1.)}$$

where $\sigma = \frac{R}{R+H_p}$. The second sum in Equation (A.1.) can be evaluated as

$$h'_\infty \sum_{n=N+1}^{\infty}\sigma^{n+1}P_n(\cos\psi_{pq}) = h'_\infty\left[\sum_{n=0}^{\infty}\sigma^{n+1}P_n(\cos\psi_{pq}) - \sum_{n=0}^{N}\sigma^{n+1}P_n(\cos\psi_{pq})\right]. \quad \text{(A.2.)}$$

Because (Moritz 1980)

$$\sum_{n=0}^{\infty}\sigma^{n+1}P_n(\cos\psi_{pq}) = \sigma\sum_{n=0}^{\infty}\sigma^{n}P_n(\cos\psi_{pq}) = \frac{\sigma}{\sqrt{1-2\sigma\cos\psi_{pq}+\sigma^2}}, \quad \text{(A.3.)}$$

we have

$$U(H_p, \psi_{pq}) = \frac{R}{M}\left[\sum_{n=0}^{N}\sigma^{n+1}h'_n P_n(\cos\psi_{pq}) + h'_\infty\sum_{n=0}^{\infty}\sigma^{n+1}P_n(\cos\psi_{pq}) - h'_\infty\sum_{n=0}^{N}\sigma^{n+1}P_n(\cos\psi_{pq})\right] \\ = \frac{R}{M}\left[\frac{h'_\infty\sigma}{\sqrt{1-2\sigma\cos\psi_{pq}+\sigma^2}} + \sum_{n=0}^{N}\sigma^{n+1}(h'_n - h'_\infty)P_n(\cos\psi_{pq})\right], \quad \text{(A.4.)}$$

which is the expression used for computations. If $H_p = 0$, then $\sigma = 1$, and the infinite series in Equation (A.3.) becomes $\frac{1}{2\sin(\psi_{pq}/2)}$. Then, we have

$$U(\psi_{pq}) = \frac{R}{M}\left[\frac{h'_\infty}{2\sin(\psi_{pq}/2)} + \sum_{n=0}^{N}(h'_n - h'_\infty)P_n(\cos\psi_{pq})\right]. \quad \text{(A.5.)}$$

The Green's function for the horizontal component of displacement can be expressed as

$$V(H_p, \psi_{pq}) = \frac{R}{M}\sum_{n=1}^{\infty}\sigma^{n+1}l'_n\frac{\mathrm{d}P_n(\cos\psi_{pq})}{\mathrm{d}\psi} \\ = \frac{R}{M}\left[\sum_{n=1}^{N}\sigma^{n+1}l'_n\frac{\mathrm{d}P_n(\cos\psi_{pq})}{\mathrm{d}\psi} + \sum_{n=N+1}^{\infty}\sigma^{n+1}l'_n\frac{\mathrm{d}P_n(\cos\psi_{pq})}{\mathrm{d}\psi}\right]. \quad \text{(A.6.)}$$

Again, for $n \geq N$ we assume $l'_n = l'_\infty =$ a constant. Then, the second term in Equation (A.6.) becomes

$$\sum_{n=N+1}^{\infty}\sigma^{n+1}l'_n\frac{\mathrm{d}P_n(\cos\psi_{pq})}{\mathrm{d}\psi} = l'_\infty\left[\sum_{n=0}^{\infty}\sigma^{n+1}\frac{\mathrm{d}P_n(\cos\psi_{pq})}{\mathrm{d}\psi} - \sum_{n=1}^{N}\sigma^{n+1}\frac{\mathrm{d}P_n(\cos\psi_{pq})}{\mathrm{d}\psi}\right]. \quad \text{(A.7.)}$$

Because

$$\sum_{n=0}^{\infty}\sigma^{n+1}\frac{\mathrm{d}P_n(\cos\psi_{pq})}{\mathrm{d}\psi} = \sigma\frac{\mathrm{d}}{\mathrm{d}\psi_{pq}}\left[\sum_{n=0}^{\infty}\sigma^{n}P_n(\cos\psi_{pq})\right] = \frac{-\sigma^2\sin\psi_{pq}}{\left(1-2\sigma\cos\psi_{pq}+\sigma^2\right)^{3/2}}, \quad \text{(A.8.)}$$

we have

$$V(H_p, \psi_{pq}) = \frac{R}{M}\left[\frac{-l'_\infty\sigma^2\sin\psi_{pq}}{\left(1-2\sigma\cos\psi_{pq}+\sigma^2\right)^{3/2}} + \sum_{n=1}^{N}\sigma^{n+1}(l'_n - l'_\infty)\frac{\mathrm{d}P_n(\cos\psi_{pq})}{\mathrm{d}\psi}\right], \quad \text{(A.9.)}$$

which is the expression for computing the Green's function. If $H_p = 0$, $\sigma = 1$, the expression in Equation (A.8.) reduces to $\frac{-\cos(\psi_{pq}/2)}{4\sin^2(\psi_{pq}/2)}$ and

$$V(\psi_{pq}) = \frac{R}{M}\left[\frac{-l'_\infty\cos(\psi_{pq}/2)}{4\sin^2(\psi_{pq}/2)} + \sum_{n=1}^{N}(l'_n - l'_\infty)\frac{\mathrm{d}P_n(\cos\psi_{pq})}{\mathrm{d}\psi}\right]. \quad \text{(A.10.)}$$